http://www.jstage.jst.go.jp/browse/biophysics

BIOPHYSICS

Vol. 9, pp. 149–159 (2013)
doi: 10.2142/biophysics.9.149

Single molecule FRET observation of kinesin-1's head-tail interaction on microtubule

Takahiro Aoki[1], Michio Tomishige[1] and Takayuki Ariga[1]

[1]*Department of Applied Physics, School of Engineering, the University of Tokyo, Tokyo, 113-8656, Japan*

Received August 19, 2013; accepted October 17, 2013

Kinesin-1 (conventional kinesin) is a molecular motor that transports various cargo such as endoplasmic reticulum and mitochondria in cells. Its two head domains walk along microtubule by hydrolyzing ATP, while the tail domains at the end of the long stalk bind to the cargo. When a kinesin is not carrying cargo, its motility and ATPase activity is inhibited by direct interactions between the tail and head. However, the mechanism of this tail regulation is not well understood. Here, we apply single molecule fluorescence resonance energy transfer (smFRET) to observe this interaction in stalk-truncated kinesin. We found that kinesin with two tails forms a folding conformation and dissociates from microtubules, whereas kinesin with one tail remains bound to the microtubule and is immobile even in the presence of ATP. We further investigated the head-tail interaction as well as head-head coordination on the microtubule at various nucleotide conditions. From these results, we propose a two-step inhibition model for kinesin motility.

Key words: molecular motor, smFRET, autoinhibition, tail-regulation, cargo transport

Kinesin-1 (conventional kinesin; hereafter called kinesin) is a motor protein that hydrolyzes ATP to transport membranous vesicles, mitochondria and other organelles along microtubules (MT) in cells[1,2]. It consists of two heavy chains and two light chains[3,4]. The heavy chains are responsible for ATP hydrolysis and MT binding. Each heavy chain is divided into four domains including a motor catalytic core (head), a short peptide linker connecting the two heads (neck linker), three coiled coil regions interrupted by two flexible hinges that ensure dimer formation (stalk) and a tail domain (tail) which associates with the cargo to be transported (Fig. 1A). A kinesin moves unidirectionally along MT by alternating its two heads in a bipedal manner (akin to walking) for several micrometers[5–7]. In cells, kinesin transports a cargo by binding to it via the tail domain and in some cases adapter proteins[8,9]. At the same time, this motility is strictly regulated to prevent futile ATP consumption (i.e. ATP consumption when no cargo is bound) and to transport cargo to the proper destination (i.e. to the axon or to dendrite of a neuron)[2,10,11].

To prevent futile ATP consumption, the motility of kinesin is inhibited by the interaction between the tail and head. When kinesin does not carry a cargo, it takes a compact folded conformation[12], which inhibits both the ATPase activity[13,14] and motility[15,16]. Numerous biochemical studies have shown that this conformation is the result of direct interaction between the conserved IAK region of the tail and the head, which inhibits both basal and MT-stimulated ADP release from the head[14,17–22]. Furthermore, it has been reported that one tail is sufficient for the inhibition[21]. Details of this inhibition are seen in X-ray crystal structures where a single tail peptide that includes the IAK region cross-links both heads near the plus-end-oriented tip (toe) position[23].

In addition to the tail-head interaction, interaction between the tail and MT is also reported[17]. Using cryo-electron microscopy, Dietrich *et al.* demonstrated that the tail peptide binds to both the nucleotide pocket of the head and MT simultaneously[24]. X-ray crystal structures, however, have

Abbreviations: MT, microtubule; smFRET, single-molecule fluorescence resonance energy transfer; 1HB, one-head-bound; 2HB, two-head-bound; CLM, cysteine-light mutant; PEG, polyethylene glycol

Corresponding author: Takayuki Ariga, Department of Applied Physics, School of Engineering, the University of Tokyo, Tokyo 113-8656, Japan. e-mail: ariga@ap.t.u-tokyo.ac.jp

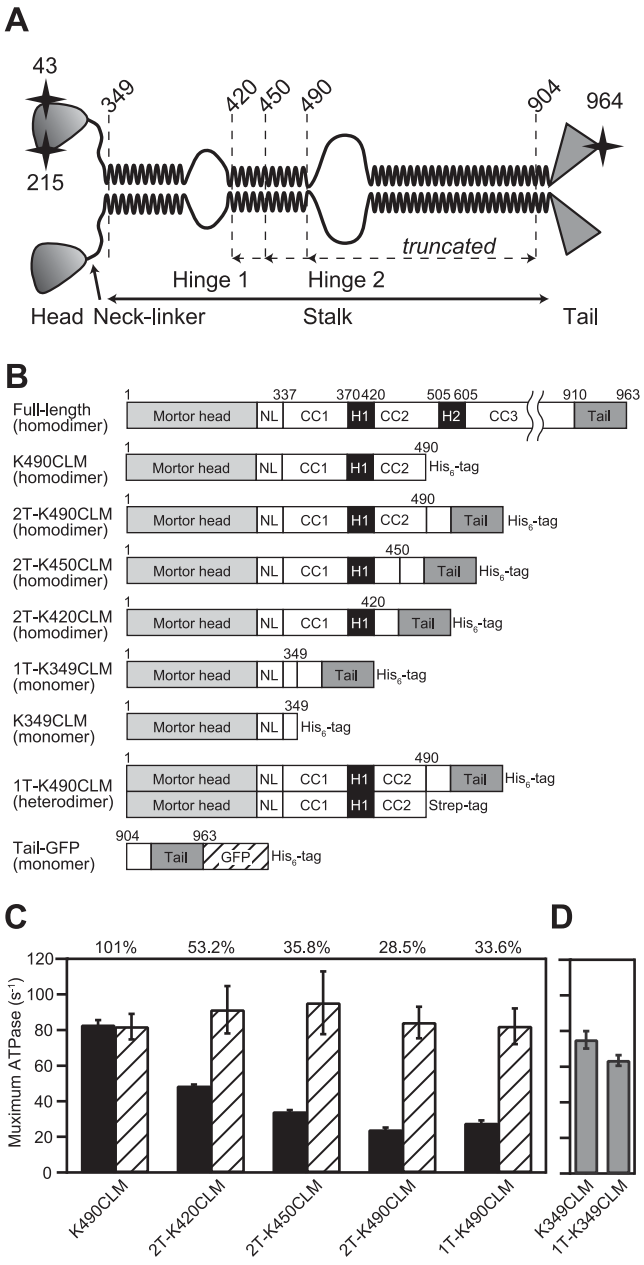

Figure 1 Kinesin constructs and their ATPase activity. (A) A schematic drawing of the full-length kinesin heavy chain dimer. The three coiled coil regions are represented by the oscillating lines. Stars denote the position of the introduced cysteine residues used for dye labeling. Dashed lines indicate the truncated regions. (B) Schematic representation of the stalk-truncated kinesin constructs. Full-length kinesin consists of a motor head, neck-linker (NL), three coiled-coil regions (CC1–CC3), two hinges (H1, H2) and tail. Stalk-truncated kinesin constructs are variably truncated at the end of the stalk region. GFP was fused to the C-terminus of the tail construct (904–963), as too was a His_6-tag (or Strep-tag). Mutations are omitted in the schematics. (C) MT-stimulated ATPase activity of dimer constructs bound or unbound to cargo. Maximum ATPase (k_{cat}) was determined from Michaelis-Menten fits to the MT-stimulated ATPase activities versus MT concentrations at 1 mM ATP, 25°C. *Solid bar* represents k_{cat} without cargo, *shaded bar* represents k_{cat} with cargo (kinesin:cargo = 1:6). *Percentages* indicate the inhibition ratio (k_{cat} without cargo)/(k_{cat} with cargo). (D) MT-stimulated ATPase activity of monomer constructs (without cargo). Error bars represent ± SE.

shown the tail interacts with the tip of the head (toe), a region distinct from the nucleotide pocket[23]. Recent studies using isolated kinesin tail peptides have reported that the tail fragment associates with MT in a manner similar to the MT-associated protein Tau[25], and that the tail fragment binds to MT at low ionic strength and inhibits head-MT interactions both in vitro[19] and in vivo[26]. Yet despite these many reports, little is known about the three-body interaction between the head, tail and MT or the dynamics of the tail regulation.

Single-molecule fluorescence resonance energy transfer (smFRET) has been used to study the dynamics of the coordination between the two heads in tail-less kinesin[27,28]. We have revealed that kinesin alternates its two heads on the MT by coupling different nucleotide-binding states as follows[28]: kinesin waits to bind ATP in the one-head-bound (1HB) state, in which the detached head bound to ADP is positioned behind the nucleotide-free leading head bound to MT; when ATP binds to the leading head, the detached head binds to the forward binding site of the MT, releasing ADP and resulting in the two-head-bound (2HB) state; finally, when the rear head hydrolyzes ATP to ADP, it detaches from the MT and kinesin returns to the 1HB state.

Here, to elucidate the conformational states of the head and tail during kinesin motility, we apply smFRET to tail-conjugated kinesin constructs. First, we engineered kinesin with partially truncated stalks and confirmed tail-mediated regulatory activities. Next, we investigated head-tail interactions in the presence or absence of MT. Comparing these results with previous ones of the two heads, we propose a two-step inhibition model for the tail regulation of kinesin in which one tail binds to the detached head to stop the motility.

Materials and Methods

DNA cloning and purification

The tail domain of human ubiquitous kinesin with a short coiled-coil region (residues 904–963) was connected to the C-terminus of 'cysteine-light' mutant (CLM) kinesin[27–30] of various stalk lengths (Fig. 1B). These constructs are designated *n*T-K*xxx*CLM, where *n* indicates the number of connected tails and *xxx* indicates the number of amino acids excluding those in the tail. Each homodimer construct contained a C-terminal His_6 tag (GTHHHHHH), whereas for heterodimers, a co-expression vector carrying two kinesin heavy chains connecting the His_6 and Strep tags (GTAWRHPQFGG) was constructed. Cysteine residues (S43C, E215C, T324C, E487C and/or 964C at C-terminus) were introduced into the constructs for dye labeling. Tail-GFP was obtained by directly connecting an EGFP gene containing a C-terminal His_6 tag into the C-terminus of the tail (904–963). All constructs were confirmed by DNA sequencing. DNA cloning, protein expression, purification and dye labeling with Cy3 and/or Cy5 were carried out as

previously described[28]. Preparation of MT and axonemes were done also as described[28].

Preparation of casein-coated beads

Casein-coated beads were used as artificial cargo and prepared as previously described[15,31] with some modification. Carboxylate-polystylene beads of diameter 0.21 µm (Polysciences, Inc. Washington, PA) were incubated in casein solution (2 mg/ml casein and 10 mM tris(hydroxymethyl) aminomethane-HCl at pH 8.0) overnight. The casein-coated beads were stored at 4°C for at least one day and were washed with BRB12 buffer (12 mM piperazine-1,4-bis(2-ethanesulfonic acid (PIPES)-KOH at pH 6.8, 2 mM $MgCl_2$ and 1 mM EGTA) to remove unbound casein just before use.

ATPase measurements

MT-stimulated ATPase activity was measured using the Malachite Green assay[15,31]. 0.1–1 nM of kinesin was mixed with various concentrations of MT in assay buffer (80 mM PIPES-KOH at pH 6.8, 1 mM $MgCl_2$, 1 mM EGTA, 1 mM DTT, 1 mg/ml casein and 1 mM ATP) and incubated for 10–40 min at 25°C. To measure the cargo state, casein-coated beads and kinesin were mixed at a 6 : 1 molar ratio. The production of phosphate was determined from the absorbance at 620 nm using the malachite green phosphate detection kit (R&D systems, MN, USA). Plots of the ATPase activity (per dimeric kinesin molecule) versus tubulin concentration were fitted to the Michaelis–Menten equation using IgorPro 6.12A (Wavemetrics, Lake Oswego, OR, USA) to obtain maximum MT-stimulated ATPase activity (k_{cat}).

Single-molecule imaging

Individual fluorescently-labeled kinesin moving along sea-urchin sperm axonemes were visualized using custom-built total internal reflection fluorescence microscopy[27,28,30]. Because the tail tends to be adsorbed to the casein-coated glass surface[32], we used a polyethylene-glycol (PEG)-coated glass surface and κ-casein to prevent nonspecific adsorption as previously describe[33–36] with some modifications (Fig. 2A).

A flow cell was constructed between KOH-cleaned or Poly-L-lysine-coated quartz slide glass[37] and a coverslip by placing a polyester spacer of 50 µm thickness in between.

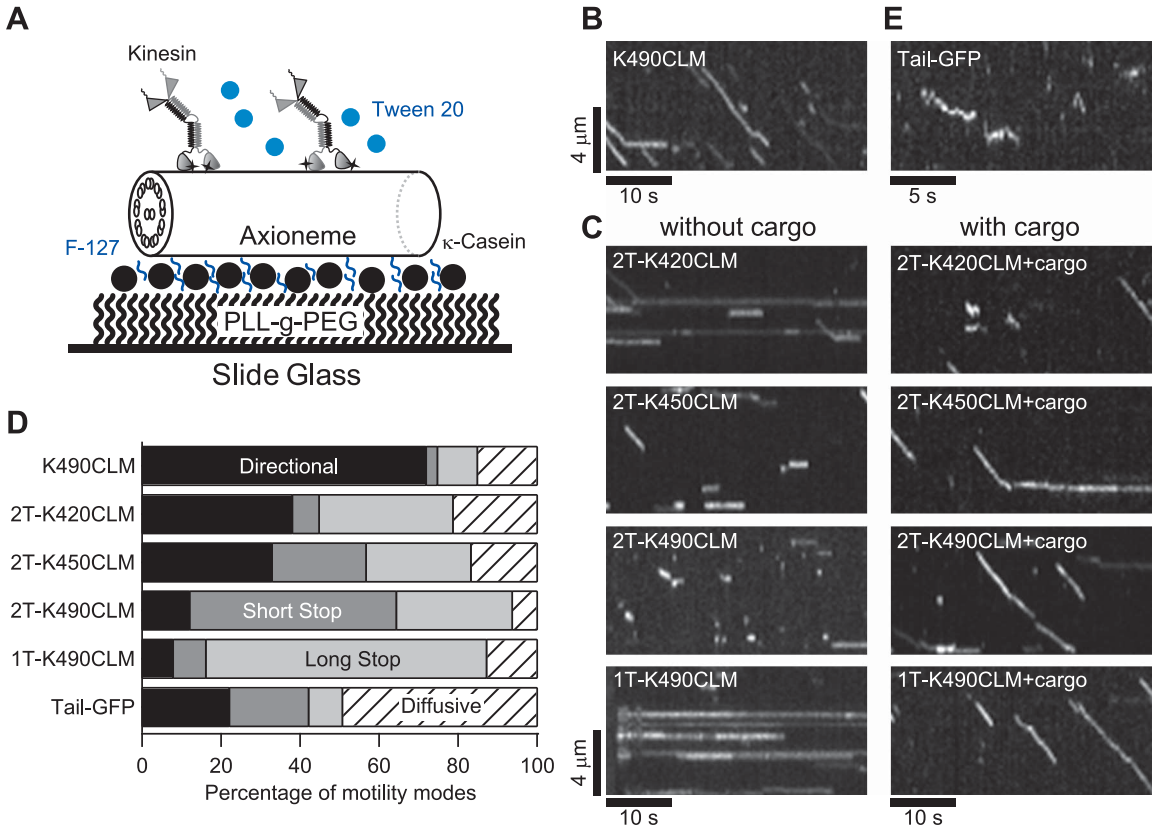

Figure 2 Kinesin motility. (A) Schematic representation of the experimental setup for single-molecule imaging of kinesin motility (not to scale). PLL-g-PEG (*black wavy lines*), κ-casein (*black spheres*), Pluronic F-127 (*blue-short wavy lines*) and Tween 20 (*blue spheres*) were used to prevent nonspecific adsorption of the tail to the glass surface. An axoneme is fixed nonspecifically to the PLL-g-PEG coated glass surface. (B) Typical kymograph for the tail-less construct K490CLM. (C) Typical kymographs for each tail-conjugated construct without (*left*) and with (*right*) cargo (kinesin:cargo = 1:6). Movements were observed at 1 mM ATP, 22°C. Scale bar, 4 µm (vertical), 10 s (horizontal). (D) Proportion of the motility modes for each construct (n = 178–459). See text for definitions of modes. (E) Typical kymograph for tail-GFP. Scale bar, 4 µm (vertical), 5 s (horizontal).

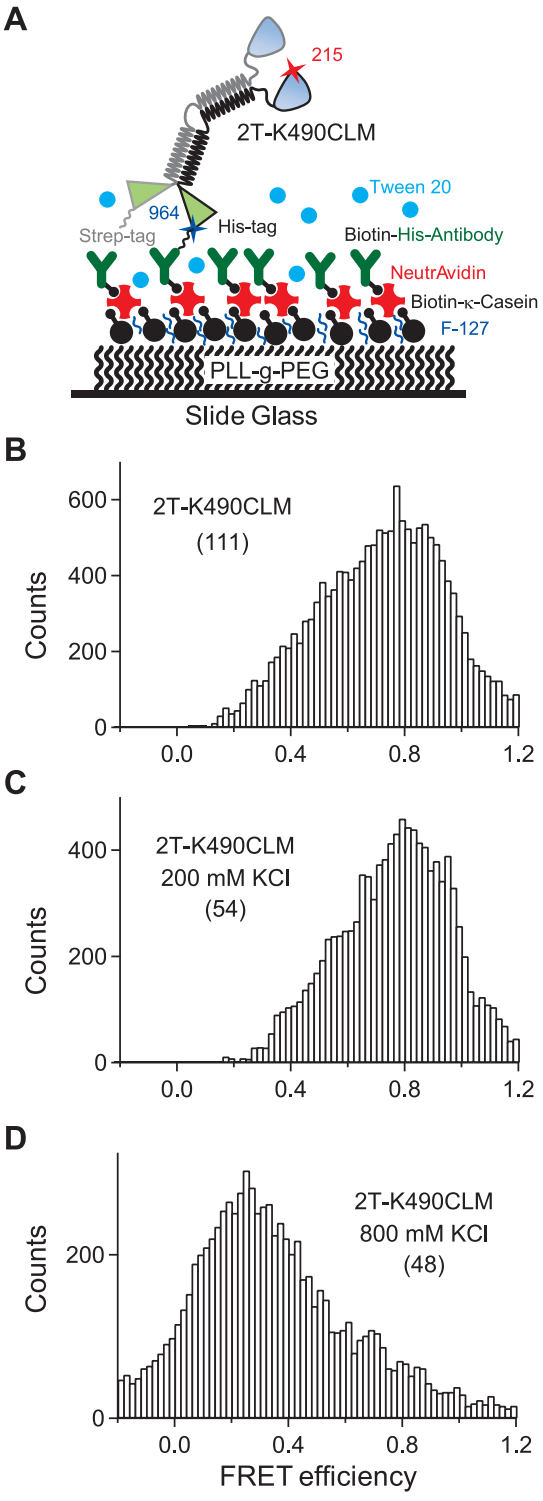

Figure 3 SmFRET observations of the head-tail interaction in two-tail kinesin. (A) Scheme of the experimental geometry for smFRET observations of 2T-K490CLM with the 215–964 sensor (not to scale). His_6-tagged kinesin is fixed onto the glass surface via a penta-His antibody (*Y shape*) immobilized with biotin-Neutravidin linkages. (B) Histograms of smFRET efficiencies from each frame of the images. (C) 2T-K490CLM smFRET efficiencies at 200 mM KCl and (D) at 800 mM KCl. Values in parentheses are the number of analyzed molecules.

The flow cell was filled with 1 mg/ml poly-l-lysine–graft–polyethylene glycol copolymers (PLL-g-PEG; SurfaceSolutionS, Zurich, Switzerland) in BRB12 buffer for over 30 min. The PEG-coated flow cell was stored in a closed container and used within a week. Just before the imaging, 0.5% (w/v) Pluronic F-127 (Anaspec, Inc., Fremont, CA, USA) and 50 µg/ml κ-casein was infused into the flow cell and incubated for 5 min, and the cell was washed with BRB12 buffer. The axoneme solution was then infused, incubated for 15 min to fix nonspecifically onto the PEG-coated glass slide and washed with BRB12 buffer. Fluorescence imaging was started after infusing 10–50 pM of dye-labeled kinesin in motility buffer (12 mM PIPES-KOH at pH 6.8, 2 mM $MgCl_2$, 1 mM EGTA, 0.1% Tween 20, 50 µg/ml κ-casein, 4.5 mg/ml glucose, 50 U/ml glucose oxidase, 50 U/ml catalase, 0.5% β-mercaptoethanol and 1 mM ATP) at 22°C. To image cargo transport, the casein-coated beads were mixed with kinesin at a 6 : 1 molar ratio and incubated for 10 min before observation.

Fluorescent dyes were illuminated with a solid state diode laser (635 nm for Cy5; Cube 635-25C, Coherent Inc.) and argon laser (514 nm for Cy3 and 488 nm for tail-GFP; 35LAP321, Melles Griot). Fluorescence images were captured by an electron-multiplying charge-coupled device camera (EM-CCD; iXon DV860 DCS-BV, Andor, USA). Image processing and data analysis were performed as previously described[28,30].

SmFRET of two-tail kinesin

SmFRET measurements of dye-labeled kinesin were performed as previously described[27,28]. However, because 2T-K490CLM bindings to MT were too short for imaging (See Results), it was imaged after being specifically immobilized onto the glass surface as follows (Fig. 3A). Penta-his antibody (Qiagen, USA) and κ-casein in BRB12 buffer were mixed with succinimidyl-6-(biotinamido)hexanoate (NHS-LC-Biotin; Pierce, Rockfold, IL, USA) in DMSO at a 2:1 molar ratio and incubated for 1 h on ice for biotinylation. 0.5% (w/v) Pluronic F-127 and 50 µg/ml biotinylated κ-casein were infused into the PEG-coated flow cell as described above, incubated for 5 min and washed with BRB12 buffer. Then, 50 µg/ml Neutravidin (Pierce, USA) in BRB12 buffer was infused into the cell, incubated for 10 min and washed with BRB12 buffer. 20 µg/ml biotinylated penta-His antibody was infused, incubated for 10 min and washed with BRB12 buffer. Dye-labeled kinesin in motility buffer, which included different concentrations of KCl (See Fig. 3), were infused and imaged at 22°C. Fluorescence images from the labeled dyes of Cy3 and Cy5 were separated by a DV2 Dual-View system (Photometrics, Tucson, AZ, USA) and captured by the EM-CCD camera. Image processing and data analysis were performed as previously described[28].

SmFRET of one tail kinesin

SmFRET measurements of the 1T-K490CLM were performed as previously described[27,28] expect for the PEG-coated flow cell and κ-casein, which were used to prevent nonspecific adsorptions of the tail as described above. Dye-labeled one-tail kinesin molecules were imaged along sea-urchin axonemes in motility buffer at 22°C. To fix the kinesin nucleotide-binding state, 75 nM ADP with 5 U/ml hexokinase or 50 U/ml apyrase were used instead of 1 mM ATP. Image processing and data analysis were performed[28].

Results

ATPase activity of stalk-truncated kinesin

To adopt smFRET for the observation of head-tail interactions, recombinant tail-conjugated CLM kinesin is required[27–30]. However, conventional E-coli expression systems can only produce impractically little purified recombinant full-length kinesin. Therefore, to express a CLM construct that includes the tail, we engineered a series of tail-conjugated kinesin of various truncations at the stalk region (Fig. 1A, B). The tail domain plus only a short fragment at the end of the coiled-coil region (residues 904–963) was connected to the C-terminus of the stalk-truncated kinesin at the indicated residue numbers in Figure 1A and B. Hereafter, we define the number of amino acids of the stalk-truncated kinesin including the N-terminus head domain as the stalk length. Whereas full-length kinesin requires hinge 2 for the compact folded conformation[15,16], our stalk-truncated kinesin molecules were designed to bend at hinge 1.

To confirm the tail-regulation potential of each construct, we measured the MT-activated ATPase activity in the presence and absence of casein-coated polystyrene beads, which acted as artificial cargo (Fig. 1C). Without cargo, the ATPase activity decreased dramatically with stalk length ($k_{cat} = 48.6 \pm 0.8\ s^{-1}$ for 2T-K420CLM, $34.1 \pm 1.0\ s^{-1}$ for 2T-K450CLM and $24.0 \pm 1.3\ s^{-1}$ for 2T-K490CLM). By contrast, all tail-conjugated kinesin with artificial cargo showed approximately equal ATPase activity (k_{cat}) of 84.2–95.3 s^{-1}, which also approximates that of tail-less kinesin, K490CLM ($81.9 \pm 7.2\ s^{-1}$). On the other hand, the monomeric tail kinesin 1T-K349CLM, in which the neck-linker links directly to the tail domain, showed almost the same ATPase rate, $63.5 \pm 3.0\ s^{-1}$, as K349CLM ($75.0 \pm 4.9\ s^{-1}$) despite the absence of cargo (Fig. 1D). These results indicate that the tail inhibition requires a certain length of the stalk coiled-coil region and at least one hinge region. We defined the inhibition ratio as the ATPase activity without cargo divided by that with cargo. 2T-K490CLM showed an inhibition ratio of 28.5% (Fig. 1C), which approximates the ratio previously reported for full length kinesin (31.8%)[15]. These results indicate that stalk-truncated kinesin can regulate its ATPase activity through its tail presumably via bending in the hinge 1 region and that 2T-K490CLM has a sufficient stalk length for interactions between the head and tail.

Motility of stalk-truncated kinesin

We next observed the movements of kinesin constructs by single-molecule imaging (Fig. 2). To reduce nonspecific interactions between the tail and the glass surface, we utilized κ-casein, Pluronic F-127, Tween 20 and PLL-g-PEG coated glass slides (Fig. 2A). Fluorescent cyanine dyes (Cy3 and/or Cy5) were introduced at the substituted cysteine residues 43 and/or 215, locations. Tail-less kinesin K490CLM showed many moving spots on MT (Fig. 2B). On the other hand, without cargo, 2T-K420CLM and 2T-K450CLM only sometimes moved, while 2T-K490CLM was virtually motionless (Fig. 2C *left*). These results indicate that tail-conjugated kinesin with sufficient stalk length can inhibit motility and that, in the inhibited state, they show impaired interactions with MT. In the presence of an artificial cargo, however, all tail-conjugated kinesin moved on the MT (Fig. 2C *right*) in manner similar to tail-less kinesin K490CLM without cargo (Fig. 2B). These results indicate that the tail of stalk-truncated kinesin can interact with the cargo and that in such a state the kinesin is active and are consistent with previous findings of full-length kinesin[15,16]. In addition, we also observed motility using the 215–964 sensor. These results confirmed tail regulation even when FRET fluorescent dyes were attached to kinesin.

The data in Figure 2B and Figure 2C *left* indicate a variety of motility modes: a proportion of kinesin molecules moved smoothly, some molecules were static, and a few showed diffusive movement. To analyze these observations quantitatively, we classified the modes of movement into four categories: directional, short stop, long stop and diffusive. The percentage of each mode is shown in Figure 2D. Bright spots with ≤100 nm/s average velocity and <2 s duration time were classified as short stop (*dark gray bar*), those with ≤80 nm run length were classified as long stop (*light gray bar*), those with ≤100 nm/s average velocity were classified as diffusive (*shaded bar*), and all others were classified as directional (*solid bar*). The percentage of the directional mode (*solid bar*) gradually decreased as stalk length increased. At the same time, the percentage of the stop modes (short stop and long stop, *dark and light gray bars*, respectively) increased. Most tail kinesin with the K490 stalk length were classified as stop mode, indicating the tail inhibits motility. Although these categories do not reflect the binding ability to MT, the binding frequencies of each construct are not so different considering they depended on the variability of PEG-coated glass surface (*data not shown*). Thus, over half of the spots of 2T-K490CLM are classified as short stop mode (52.3%) with a duration time of 1.47 ± 0.05 s, which indicates a low affinity for MT, consistent with reports on full-length kinesin[16]. These observations also argue that the 2T-K490CLM stalk length is sufficient for regulating the motility and that the head and tail domains of 2T-K490CLM can interact, consistent with ATPase measurements (Fig. 1C). Thus, we used truncated kinesin with a stalk length of 490 amino acids for the inves-

tigation of head-tail interactions.

ATPase activity and motility of one-tail kinesin

Hackney *et al.* have reported that only one monomeric tail peptide is sufficient for regulating the ATPase activity of dimeric heads in the absence of MT[21,23]. To test whether only one tail domain can inhibit the ATPase and motility, we measured the MT-stimulated ATPase activity and motility of heterodimeric 1T-K490CLM, which has only one tail domain and a stalk sufficiently long for head-tail interactions. 1T-K490CLM had almost the same MT-stimulated ATPase activity with and without cargo ($82.1\pm10.0\,s^{-1}$ and $27.6\pm1.6\,s^{-1}$, respectively) as 2T-K490CLM ($84.2\,s^{-1}$ and $24.0\,s^{-1}$, respectively; Fig. 1C). The inhibition rate of 1T-K490CLM (33.6%) was also similar to that of 2T-K490CLM (28.5%; Fig. 1C) as well as full-length kinesin (31.8%)[15]. Single-molecule imaging of kinesin with cargo showed 1T-K490CLM moves on MT (Fig. 2C *right*) in manner similar to tail-less kinesin K490CLM (Fig. 2B). Without cargo, however, 71.1% of 1T-K490CLM interacted with MT in the long stop mode and had a dwell time ≥ 2 s, which is a percentage significantly higher than that of 2T-K490CLM (29.3%) (Fig. 2C *left*, Fig. 2D). These results indicate that 1T-K490CLM can inhibit the ATPase activity and motility by binding to the MT strongly and taking the inhibited state.

Interaction between free tail and MT

To test how a free tail interacts with MT, we also observed the movement of tail-GFP fusion proteins on MT using single-molecule imaging (Fig. 2E). Approximately half of tail-GFP (49.3%) showed the diffusive mode with a duration time of 1.73 ± 0.10 s (Fig. 2D). Although ensemble measurements have shown that the tail domain can bind tightly to MT[17,25], our single-molecule results give greater detail of the interaction, showing the tail interacts with MT weakly via repeated bindings and dissociations.

SmFRET observation of two-tail kinesin

Single-molecule imaging revealed that 2T-K490CLM weakly interacts with MT (Fig. 2C *left*). To investigate its head-tail interactions when unbound to MT, we carried out smFRET observations of 2T-K490CLM captured on a penta-His antibody-coated slide glass via the His_6 tag of the C-terminus of the construct (Fig. 3A).

To validate our experimental setup, we measured the smFRET efficiencies of two control constructs that contain smFRET sensors separated by long or short distances (Supplementary Fig. S1A). K490CLM has a 215–487 sensor, where one cysteine residue is in the toe of the head (residue 215) and the other is at the end of the stalk (residue 487) such that the sensors are separated by over 10 nm. K349CLM has a 215–324 sensor, where one cysteine residue is in the toe of the head and the other is in the middle of the neck-linker such that their distance is about 2 nm when in the ADP-bound state according to crystal structures[38]. Typical traces of the fluorescence intensities of the constructs and the corresponding smFRET efficiencies are shown in Supplementary Figure S1B. These traces indicate low and high smFRET efficiencies for K490CLM and K349CLM, respectively, with single peaks at about 10% and 80% (Supplementary Fig. S1C).

To examine head-tail interactions of 2T-K490CLM, we introduced the 215–964 sensor where again one cysteine residue is in the toe of the head (residue 215) and the other is at the C-terminus of the tail domain (residue 964) for the labeling of Cy3 (donor) and Cy5 (acceptor) on the same heavy chain (Fig. 3A). SmFRET efficiency showed a single peak at about 80% (Fig. 3B), which demonstrates interaction between the tail and head.

At 800 mM KCl, full-length kinesin show unfolded conformations and rapidly release ADP[12,20]. To confirm this behavior is sensitive to ionic strength, we measured the smFRET efficiency of 2T-K490CLM at 200 and 800 mM KCl, finding peaks at 80% and 20%, respectively (Fig. 3C, D). These results confirm that the head-tail interactions are impaired at high ionic strength, but can take the folded conformation to inhibit kinesin activity at physiological conditions (ionic strength ~100 mM KCl), as previously reported[12,20].

SmFRET observation of one-tail kinesin

Unlike two-tail kinesin, we found that 1T-K490CLM binds tightly to MT in the inactive state (Fig. 2C), indicating that one tail domain can interact with at least one head domain to inhibit kinesin activity. To investigate how this inhibition occurs, we observed the head-tail interaction and the head-head coordination using smFRET[28].

First, to probe the two-head configuration in the inactive state of 1T-K490CLM, we measured smFRET efficiencies using the 215–43 sensor, where one head contains a cysteine residue in the toe of the head (residue 215) and the other contains a cysteine residue in the heel of the head (residue 43) (Fig. 4A). At 50 U/ml apyrase, which represents the no-nucleotide binding state, smFRET efficiencies showed a bimodal distribution with peaks at about 10% and 90%. This result is very similar to that previously observed using the tail-less kinesin K490CLM[28], indicating that 1T-K490CLM is in the 2HB state when no nucleotide is bound. Although tail-less kinesin interacts stably with MT in the 1HB state at 200 nM ADP[28], our experiments did not find 1T-K490CLM could do the same (*data not shown*). At 75 nM ADP, however, 1T-K490CLM did bind to MT, and its smFRET efficiency had a single peak at 40%, while tail-less kinesin K490CLM had one at ~30%, indicating 1T-K490CLM is in the 1HB state[28]. Results at 1 mM ATP, where 1T-K490CLM binds to MT and is immobilized, were similar to those at 75 nM ADP, indicating that the motility of 1T-K490CLM is inhibited by one tail in almost the same conformational 1HB state as at 75 nM ADP.

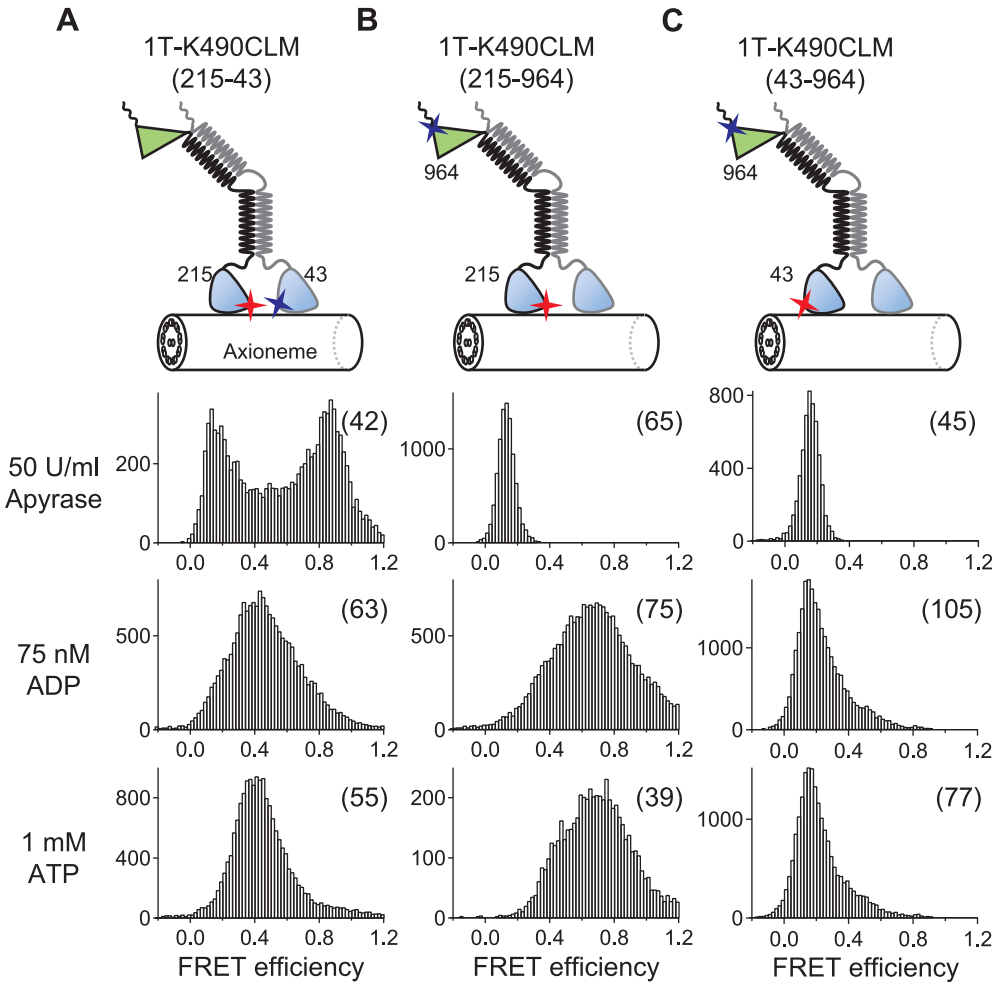

Figure 4 SmFRET observations of the head-head configuration and head-tail interaction in one-tail kinesin. (A) Histograms of smFRET efficiencies (from each frame) for the 215–43 sensor of 1T-K490CLM, (B) 215–964 sensor of 1T-K490CLM and (C) 43–964 sensor of 1T- K490CLM at 50 U/ml apyrase (*top*), 75 nM ADP (*middle*) and 1 mM ATP (*bottom*). Values in parentheses are the number of analyzed molecules.

To examine the interactions between the tail and two heads when kinesin is bound to MT, we measured smFRET efficiency using the 215–964 sensor of 1T-K490CLM (Fig. 4B). The smFRET efficiency showed a single high peak of ~80% at both 75 nM ADP and 1 mM ATP, but a much lower peak (~10%) at 50 U/ml apyrase (Fig. 4B). The ~10% efficiency is almost the same as the efficiency for the 215–487 sensor of tail-less kinesin K490CLM (Supplementary Fig. S1), suggesting an unbound state between the tail and head. Considering the above results of the 215–43 sensor (Fig. 4A), the 215–964 sensor results suggest the tail binds to the head in the 1HB state, but not the 2HB state.

To estimate the head-tail coordination in the inactive state, we measured smFRET efficiencies using the 43–964 sensor of 1T-K490CLM (Fig. 4C). The smFRET efficiency was almost the same as that of the 215–964 sensor at 50 U/ml apyrase, whereas it was lower than that of the 215–964 sensor (20% vs. 80%) at both 75 nM ADP and 1 mM ATP. These results indicate that in the 1HB state of the head-tail complex, the C-terminus of the tail (964) is located at the vicinity of the toe of the head (215), far from the heel of the head (43).

Discussion

Tail-mediated regulation of the stalk partially truncated kinesins

Here, we explore the head-tail interaction of kinesin using smFRET observations in the presence and absence of MT. For this purpose, we first constructed tail-conjugated kinesin of various stalk lengths (Fig. 1A, B) and measured their MT-stimulated ATPase activity and motility (Fig. 1C, Fig. 2). These results show that truncated kinesin with stalk lengths of 490 amino acids demonstrate mature tail-inhibition ability and full activation potential in the presence of a cargo. These properties are almost identical to those seen for full-length kinesin[15,16], indicating that the tail of the stalk-truncated constructs is able to interact with the head by presumably bending hinge 1, which is located mid-

way in the coiled coils of the shortened stalk. Furthermore, single-molecule imaging rarely showed the two-tail kinesin 2T-K490CLM walking along MT (Fig. 2C), which corresponds to the fact that kinesin in the inhibited state floats in the cytosol in vivo[4,26]. The lower binding affinity for MT is probably because the kinesin tail inhibits the release of ADP from the head[17]. On the other hand, we found that 1T-K490CLM, which conjugates only one tail, bound strongly to MT even in the presence of ATP even though the ATPase activity and motility were inhibited. This finding implies the existence of an intermediate state in which the tail inhibits kinesin motility.

Dissociation of kinesin heads from MT requires the interaction of both tails with both heads

We show that two-tail kinesin can dissociate from MT, whereas for one-tail kinesin at least one head is always bound to MT even in the presence of ATP (Fig. 2C). Hackney *et al.* showed that one tail peptide can bind concomitantly to both heads[23] and prevents ADP release[21]. Taken together, these results suggest one tail appears sufficient to prevent MT binding and ADP release from one head, but insufficient to prevent these events from the other head. On the other hand, whereas tail-less kinesin can be in the 1HB state when bound to MT at 200 nM ADP[28], we found that one-tail kinesin requires lower ADP concentrations of 75 nM to interact with MT when no cargo is bound. This result indicates subtle differences between the free head and the tail-interacting head for MT affinity and ADP-release.

Comparison with reported structures of the head-tail complex

The distance between two probe dyes can be estimated by smFRET. SmFRET efficiency is calculated as $E_{FRET} = [1+(R/R_0)^6]^{-1}$, where R is the distance between the two sensor dyes and $R_0 = 5.3$ nm is their Förster distance assuming random dye orientation (orientation factor, $\kappa^2 = 2/3$)[39]. Here we obtained ~80% smFRET efficiency for the 215–964 sensor in the folded state (Fig. 3), which corresponds to a distance of ~4.2 nm between the toe of the head (215) and the C-terminus of the tail (964). Note that the efficiency of the 215–324 sensor in K349CLM, which according to crystal structures has a distance of ~2 nm[38], was also ~80% (Supplementary Fig. S1) implying that the ~4.2 nm distance of the 215–964 sensor might be an overestimate due to uncertainties in the orientation factor (κ^2) and R_0. On the other hand, the smFRET efficiency for the 43–964 sensor of 1T-K490CLM showed ~20% efficiency at both 75 nM ADP and 1 mM ATP, indicating an ~6.6 nm distance between the heel of the head and the C-terminus of the tail (Fig. 4C). Although these estimations are unlikely to be precise because of uncertainties in the orientation factor, we argue that the C-terminus of the tail (964) is located closer to the toe (215) of the head than the heel (43) in the inactive folded state.

X-ray crystallography studies have reported the structure of the tail-head complex[23], showing that the IAK-region peptide of the tail is located nearby the toe (215) of the head (distance: ~1 nm). Although the size of the tail is unknown, it is expected to be significantly smaller than the head (~5 nm)[40], which argues the distance between the 215–964 sensors is even less, a conclusion supported by our smFRET measurements in the tail-mediated inhibited state. On the other hand, an electron-microscopy study has reported the structure of a photochemically cross-linked tail-head complex on MT[24], finding that the C-terminus of the tail domain is near the heel (43) of the head domain, >5 nm apart from the toe (215), which corresponds to the <60% smFRET efficiency. This discrepancy might be due to the artificial cross-linking of the tail-head complex. However, because we observed a weak interaction between the tail-GFP and MT (Fig. 2E), the tail-MT contact shown by the electron-microscopy might instead reflect a weak interaction between the tail and MT.

Head-tail interaction of the one-tail kinesin bound to MT

To investigate the head-tail interaction on MT, we conducted smFRET measurements between the tail and head and between the two heads of the one-tail kinesin 1T-K490CLM while it was bound to MT (Fig. 4). The results expose several details of the head-tail interaction as follows.

First, at 50 U/ml apyrase, i.e. no-nucleotide condition, 1T-K490CLM is in the 2HB state and the tail does not interact with either head. This structural state is almost the same as the state of the tail-less kinesin[28], suggesting that the tail cannot interact with the MT-bound head in the no-nucleotide state.

Second, at low ADP concentrations, 1T-K490CLM is in the 1HB state, again like tail-less kinesin[28], such that the tail interacts with the detached head. 1T-K490CLM showed ~40% FRET efficiency when measuring the 215–43 sensor, whereas the tail-less kinesin showed ~30%[28]. This discrepancy could be reflected by a small structural change induced by the binding of the tail to the head. In fact, the crystal structure of the tail-head complex showed that the neck-linker conformation of the head is slightly changed but that the position of both heads is fixed[23] compared to that in the 1HB state of the tail-less kinesin[28], yielding different distances between the 215 (toe) and 43 (heel) residues.

Finally, at 1 mM ATP, a condition in which tail-less kinesin walks along MT, 1T-K490CLM is immobile and takes the 1HB state, where the tail interacts with the detached head, similar to the low ADP conditions described above, indicating that the other head always binds to MT even in the presence of ATP. These results suggest that the transition to the ADP state of the MT-bound head, which includes ATP binding to the head and/or ATP hydrolysis, is inhibited to prevent dissociation from the MT. Because the tail interacts with the detached head, this head cannot bind to the forward binding site on MT. As a result, ATP binding and/or

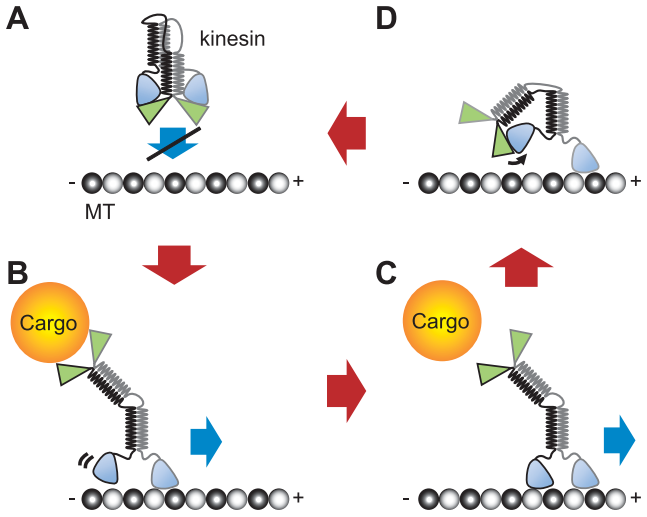

Figure 5 A two-step model for the tail regulation of kinesin. (A) Without cargo, kinesin heads cannot bind to MT due to interactions within their respective tails. (B) When a cargo binds to the tail, the interaction is relieved and kinesin binds to and walks along the microtubule. (C) When the cargo detaches from the tail, kinesin can still walk along MT. (D) Just after this detachment, one tail binds to the detached head in (C), which prevents further ATP hydrolysis and motility. The other tail then binds to the other head causing kinesin to detach from MT, returning to state (A).

ATP hydrolysis of the MT-bound head might be slowed due to inhibition of a speculated neck-linker-mediated acceleration[41,42].

Two-step inhibition model

From the above results, we propose a model for the tail inhibition of kinesin motility (Fig. 5). When kinesin is not carrying cargo, it takes the folded conformation and diffuses in the cytosol without hydrolyzing ATP (Fig. 5A). When a cargo binds to the tail, the tail releases from the head, conforming kinesin to the active state for cargo transport along the MT (Fig. 5B). Just after unloading the cargo, should the kinesin remain in the active state, it continues hydrolyzing ATP unnecessarily (Fig. 5C). To prevent this outcome, the tail binds to the detached head (Fig. 5D). Finally, the other tail interacts with the attached head to complete the folded conformation, returning us to the original state of the model (Fig. 5A). Although it is not clear how kinesin with just one tail binds strongly to MT in the presence of ATP, we found that one tail is sufficient for inhibiting the active state when kinesin does not bind cargo.

Role of kinesin light chain and cargo-binding process

Although we show that the binding and unbinding of cargo are sufficient for regulating the motility of the kinesin heavy chains and their binding to MT, the previous reports have also shown the importance of the light chains in these phenomena[4,43]. Cai *et al.* reported that the light chains are important for full-length kinesin taking the inactive state and dissociating from the MT in live cell[4]. Because many cargos such as endoplasmic reticula, mitochondria and other organelles are readily available in a living cell, we assume that the binding of cargo is sufficient for the activation of the kinesin heavy chains in the absence of the light chains. Alternatively, the weak binding of the tail to the MT (Fig. 2E) is possibly involved in the activation as previously proposed[43]. Although our model ignored the effects of cargo binding on the activation process (Fig. 5A to B), many groups have reported that activation is associated with several binding partners including the kinesin light chains[4,8,9,43]. Therefore, it may be that the kinesin heavy chains are sufficient for preventing futile ATP hydrolysis, whereas the kinesin light chains (and other partners) may be involved in the regulation of proper cargo binding. Understanding the latter regulation will be necessary for complete understanding of kinesin motility[2,10].

Conclusion

Using tail-conjugated kinesin with partially truncated stalks, we detected head-tail interactions by smFRET. The results identified a novel intermediate state in which only one tail inhibits the kinesin motility, leading us to propose a two-step inhibition model for the tail-regulation process. Such an autoinhibition mechanism has been found throughout the kinesin family[44–48] and other motor molecules[49,50]. The SmFRET approach described here is expected to be applicable for the comprehensive investigation of mechanisms regulating various cellular functions.

Acknowledgements

We thank Michiko Nakajima for support in the cloning, Teppei Mori and Yamato Niitani for the image processing program, Chikako Shingyoji for the sea urchin sperm axoneme, Peter Karagiannis for critically revising the manuscript and other Tomishige lab members for variable discussions. This work was supported in part by JSPS KAKENHI Grant Number 2118504, 25870173 (to T.A.).

REFERENCES

1. Vale, R.D. The molecular motor toolbox for intracellular transport. *Cell* **112**, 467–480 (2003).
2. Hirokawa, N., Noda, Y., Tanaka, Y. & Niwa, S. Kinesin superfamily motor proteins and intracellular transport. *Nat. Rev. Mol. Cell Biol.* **10**, 682–696 (2009).
3. Verhey, K.J., Lizotte, D.L., Abramson, T., Barenboim, L., Schnapp, B.J. & Rapoport, T.A. Light chain-dependent regulation of Kinesin's interaction with microtubules. *J. Cell Biol.* **143**, 1053–1066 (1998).
4. Cai, D., Hoppe, A.D., Swanson, J.A. & Verhey, K.J. Kinesin-1 structural organization and conformational changes revealed by FRET stoichiometry in live cells. *J. Cell Biol.* **176**, 51–63 (2007).
5. Asbury, C.L., Fehr, A.N. & Block, S.M. Kinesin moves by

an asymmetric hand-over-hand mechanism. *Science* **302**, 2130–2134 (2003).
6. Kaseda, K., Higuchi, H. & Hirose, K. Alternate fast and slow stepping of a heterodimeric kinesin molecule. *Nat. Cell Biol.* **5**, 1079–1082 (2003).
7. Yildiz, A., Tomishige, M., Vale, R. D. & Selvin, P. R. Kinesin walks hand-over-hand. *Science* **303**, 676–678 (2004).
8. Horiuchi, D., Collins, C. A., Bhat, P., Barkus, R. V., Diantonio, A. & Saxton, W. M. Control of a kinesin-cargo linkage mechanism by JNK pathway kinases. *Curr. Biol.* **17**, 1313–1317 (2007).
9. Blasius, T. L., Cai, D., Jih, G. T., Toret, C. P. & Verhey, K. J. Two binding partners cooperate to activate the molecular motor Kinesin-1. *J. Cell Biol.* **176**, 11–17 (2007).
10. Verhey, K. J. & Hammond, J. W. Traffic control: regulation of kinesin motors. *Nat. Rev. Mol. Cell Biol.* **10**, 765–777 (2009).
11. Adio, S., Reth, J., Bathe, F. & Woehlke, G. Review: regulation mechanisms of Kinesin-1. *J. Muscle Res. Cell Motil.* **27**, 153–160 (2006).
12. Hackney, D. D., Levitt, J. D. & Suhan, J. Kinesin undergoes a 9S to 6S conformational transition. *J. Biol. Chem.* **267**, 8696–8701 (1992).
13. Jiang, M. Y. & Sheetz, M. P. Cargo-activated ATPase activity of kinesin. *Biophys. J.* **68**, 283S–284S (1995).
14. Stock, M. F., Guerrero, J., Cobb, B., Eggers, C. T., Huang, T. G., Li, X. & Hackney, D. D. Formation of the compact confomer of kinesin requires a COOH-terminal heavy chain domain and inhibits microtubule-stimulated ATPase activity. *J. Biol. Chem.* **274**, 14617–14623 (1999).
15. Coy, D. L., Hancock, W. O., Wagenbach, M. & Howard, J. Kinesin's tail domain is an inhibitory regulator of the motor domain. *Nat. Cell Biol.* **1**, 288–292 (1999).
16. Friedman, D. S. & Vale, R. D. Single-molecule analysis of kinesin motility reveals regulation by the cargo-binding tail domain. *Nat. Cell Biol.* **1**, 293–297 (1999).
17. Hackney, D. D. & Stock, M. F. Kinesin's IAK tail domain inhibits initial microtubule-stimulated ADP release. *Nat. Cell Biol.* **2**, 257–260 (2000).
18. Seiler, S., Kirchner, J., Horn, C., Kallipolitou, A., Woehlke, G. & Schliwa, M. Cargo binding and regulatory sites in the tail of fungal conventional kinesin. *Nat. Cell Biol.* **2**, 333–338 (2000).
19. Yonekura, H., Nomura, A., Ozawa, H., Tatsu, Y., Yumoto, N. & Uyeda, T. Q. Mechanism of tail-mediated inhibition of kinesin activities studied using synthetic peptides. *Biochem. Biophys. Res. Commun.* **343**, 420–427 (2006).
20. Hackney, D. D. & Stock, M. F. Kinesin tail domains and Mg^{2+} directly inhibit release of ADP from head domains in the absence of microtubules. *Biochemistry* **47**, 7770–7778 (2008).
21. Hackney, D. D., Baek, N. & Snyder, A. C. Half-site inhibition of dimeric kinesin head domains by monomeric tail domains. *Biochemistry* **48**, 3448–3456 (2009).
22. Wong, Y. L., Dietrich, K. A., Naber, N., Cooke, R. & Rice, S. E. The Kinesin-1 tail conformationally restricts the nucleotide pocket. *Biophys. J.* **96**, 2799–2807 (2009).
23. Kaan, H. Y., Hackney, D. D. & Kozielski, F. The structure of the kinesin-1 motor-tail complex reveals the mechanism of autoinhibition. *Science* **333**, 883–885 (2011).
24. Dietrich, K. A., Sindelar, C. V., Brewer, P. D., Downing, K. H., Cremo, C. R. & Rice, S. E. The kinesin-1 motor protein is regulated by a direct interaction of its head and tail. *Proc. Natl. Acad. Sci. USA* **105**, 8938–8943 (2008).
25. Seeger, M. A. & Rice, S. E. Microtubule-associated protein-like binding of the kinesin-1 tail to microtubules. *J. Biol. Chem.* **285**, 8155–8162 (2010).
26. Watanabe, T. M., Yanagida, T. & Iwane, A. H. Single molecular observation of self-regulated kinesin motility. *Biochemistry* **49**, 4654–4661 (2010).
27. Tomishige, M., Stuurman, N. & Vale, R. D. Single-molecule observations of neck linker conformational changes in the kinesin motor protein. *Nat. Struct. Mol. Biol.* **13**, 887–894 (2006).
28. Mori, T., Vale, R. D. & Tomishige, M. How kinesin waits between steps. *Nature* **450**, 750–754 (2007).
29. Rice, S., Lin, A. W., Safer, D., Hart, C. L., Naber, N., Carragher, B. O., Cain, S. M., Pechatnikova, E., Wilson-Kubalek, E. M., Whittaker, M., Pate, E., Cooke, R., Taylor, E. W., Milligan, R. A. & Vale, R. D. A structural change in the kinesin motor protein that drives motility. *Nature* **402**, 778–784 (1999).
30. Tomishige, M. & Vale, R. D. Controlling kinesin by reversible disulfide cross-linking. Identifying the motility-producing conformational change. *J. Cell Biol.* **151**, 1081–1092 (2000).
31. Coy, D. L., Wagenbach, M. & Howard, J. Kinesin takes one 8-nm step for each ATP that it hydrolyzes. *J. Biol. Chem.* **274**, 3667–3671 (1999).
32. Ozeki, T., Verma, V., Uppalapati, M., Suzuki, Y., Nakamura, M., Catchmark, J. M. & Hancock, W. O. Surface-bound casein modulates the adsorption and activity of kinesin on SiO2 surfaces. *Biophys. J.* **96**, 3305–3318 (2009).
33. Bieling, P., Telley, I. A., Piehler, J. & Surrey, T. Processive kinesins require loose mechanical coupling for efficient collective motility. *EMBO Rep.* **9**, 1121–1127 (2008).
34. Valentine, M. T., Fordyce, P. M., Krzysiak, T. C., Gilbert, S. P. & Block, S. M. Individual dimers of the mitotic kinesin motor Eg5 step processively and support substantial loads in vitro. *Nat. Cell Biol.* **8**, 470–476 (2006).
35. Telley, I. A., Bieling, P. & Surrey, T. Obstacles on the microtubule reduce the processivity of Kinesin-1 in a minimal in vitro system and in cell extract. *Biophys. J.* **96**, 3341–3353 (2009).
36. Furuta, K. & Toyoshima, Y. Y. Minus-end-directed motor Ncd exhibits processive movement that is enhanced by microtubule bundling in vitro. *Curr. Biol.* **18**, 152–157 (2008).
37. Fordyce, P. M., Valentine, M. T. & Block, S. M. Advances in surface-based assays for single molecules. in *Single-molecule techniques: A laboratory manual*. (Selvin, P. & Ha, T. ed). pp. 431–460 (Cold Spring Harbor Laboratory Press. Cold Spring Harbor, NY, 2007).
38. Sindelar, C. V., Budny, M. J., Rice, S., Naber, N., Fletterick, R. & Cooke, R. Two conformations in the human kinesin power stroke defined by X-ray crystallography and EPR spectroscopy. *Nat. Struct. Biol.* **9**, 844–848 (2002).
39. Ishii, Y., Yoshida, T., Funatsu, T., Wazawa, T. & Yanagida, T. Fluorescence resonance energy transfer between single fluorophores attached to a coiled-coil protein in aqueous solution. *Chemical Physics* **247**, 163–173 (1999).
40. Hisanaga, S., Murofushi, H., Okuhara, K., Sato, R., Masuda, Y., Sakai, H. & Hirokawa, N. The molecular structure of adrenal medulla kinesin. *Cell Motil. Cytoskeleton* **12**, 264–272 (1989).
41. Yildiz, A., Tomishige, M., Gennerich, A. & Vale, R. D. Intramolecular strain coordinates kinesin stepping behavior along microtubules. *Cell* **134**, 1030–1041 (2008).
42. Clancy, B. E., Behnke-Parks, W. M., Andreasson, J. O., Rosenfeld, S. S. & Block, S. M. A universal pathway for kinesin stepping. *Nat. Struct. Mol. Biol.* **18**, 1020–1027 (2011).
43. Wong, Y. L. & Rice, S. E. Kinesin's light chains inhibit the head- and microtubule-binding activity of its tail. *Proc. Natl. Acad. Sci. USA* **107**, 11781–11786 (2010).
44. Hammond, J. W., Blasius, T. L., Soppina, V., Cai, D. & Verhey, K. J. Autoinhibition of the kinesin-2 motor KIF17 via

dual intramolecular mechanisms. *J. Cell Biol.* **189**, 1013–1025 (2010).
45. Imanishi, M., Endres, N. F., Gennerich, A. & Vale, R. D. Autoinhibition regulates the motility of the C. elegans intraflagellar transport motor OSM-3. *J. Cell Biol.* **174**, 931–937 (2006).
46. Hammond, J. W., Cai, D., Blasius, T. L., Li, Z., Jiang, Y., Jih, G. T., Meyhofer, E. & Verhey, K. J. Mammalian Kinesin-3 motors are dimeric in vivo and move by processive motility upon release of autoinhibition. *PLoS Biol.* **7**, e72 (2009).
47. Espeut, J., Gaussen, A., Bieling, P., Morin, V., Prieto, S., Fesquet, D., Surrey, T. & Abrieu, A. Phosphorylation relieves autoinhibition of the kinetochore motor Cenp-E. *Mol. Cell* **29**, 637–643 (2008).
48. Guzik, B. W. & Goldstein, L. S. Microtubule-dependent transport in neurons: steps towards an understanding of regulation, function and dysfunction. *Curr. Opin. Cell Biol.* **16**, 443–450 (2004).
49. Wang, F., Thirumurugan, K., Stafford, W. F., Hammer, J. A., 3rd, Knight, P. J. & Sellers, J. R. Regulated conformation of myosin V. *J. Biol. Chem.* **279**, 2333–2336 (2004).
50. Sellers, J. R. & Knight, P. J. Folding and regulation in myosins II and V. *J. Muscle. Res. Cell Motil.* **28**, 363–370 (2007).